RSC Advances

PAPER

View Article Online
View Journal | View Issue

Check for updates

Cite this: *RSC Adv.*, 2025, **15**, 16015

MnO_2-decorated graphene oxide nanosheet composites as promising electrode materials for lithium-ion battery energy storage applications

Yen Kim Nguyen Chuong,†[ab] Vu Van Thang,†[a] Thuy Trang Thi Vuong,[a] Phat Tan Vu,[b] Thi Viet Bac Phung,[a] Long Phi Nguyen *[a] and Phung My Loan Le *[bc]

Received 25th March 2025
Accepted 7th May 2025

DOI: 10.1039/d5ra02093j

rsc.li/rsc-advances

This study reports the synthesis of graphene oxide nanosheets (GNs) through a simple one-step electrochemical exfoliation method, followed by the decoration of manganese dioxide (MnO_2) on the GNs using a fast, straightforward wet-chemical process. The results show that MnO_2 nanosheets are uniformly dispersed on the surface of the graphene oxide, preventing the aggregation of the nanosheets. Among the samples tested, the GM005 composite exhibited the best performance, demonstrating a specific capacity of 382.1 mA h g^{-1} after 100 cycles at 0.5 A g^{-1}, making it a promising anode material for lithium-ion batteries. The enhanced electrochemical performance of the GNs@MnO_2 composite is attributed to the synergistic effect between the highly conductive graphene oxide nanosheets and flower-structure MnO_2. These findings suggest that GNs@MnO_2 could be a viable electrode material for advanced lithium-ion battery technologies.

Open Access Article. Published on 19 May 2025. Downloaded on 1/20/2026 8:11:44 AM.
This article is licensed under a Creative Commons Attribution-NonCommercial 3.0 Unported Licence.

1 Introduction

The growing demand for portable energy storage devices, fueled by technological advancements and changing societal lifestyles, has led to a surge in the disposal of outdated electronics, exacerbating the growing issue of e-waste.[1] Zinc–carbon (Zn–C) batteries, commonly used in devices like remote controls and flashlights,[2] are inexpensive power sources that utilize a graphite carbon cathode.[1] However, despite their widespread use, the majority of these batteries are not recycled, contributing to environmental concerns. Fortunately, the graphite electrode in Zn–C batteries remains inert after discharge, making it a valuable resource for reuse in various applications, such as energy storage.[2,3] One promising direction is the transformation of recycled graphite into graphene oxide nanosheets, which can serve as an advanced anode material in lithium-ion batteries (LIBs). This approach can mitigate the environmental burden of e-waste and address the performance limitations of conventional graphite anodes in LIBs.

Several chemical exfoliation methods have been developed for producing graphene oxide nanosheets (GNs) from graphite, such as the Staudenmaier, Hoffman, and Hummers methods. Each technique varies primarily in the oxidizing agents and reagent concentrations used.[1] The Staudenmaier method utilizes fuming nitric acid, concentrated sulfuric acid, and potassium chlorate, while the Hoffman method substitutes fuming nitric acid with concentrated nitric acid.[4] The Hummers' method employs concentrated sulfuric acid, sodium nitrate, and potassium permanganate.[5] Electrochemical exfoliation, as one of the excellent top-down methods, provides a promising strategy with fast and simple installation, easy control, and scalability, which gives the necessary products under adjustable conditions.[6] This method can be used with various electrolytes, including acids, salts, and bases, and produces graphene oxide nanoflakes and nanosheets with various functional groups on the surface. This allows graphene to be modified for multiple applications, including catalysts, sensors, and energy storage.[7,8]

In energy storage, GNs produced *via* electrochemical exfoliation will be utilized as anode materials in LIBs. Due to their high energy density, LIBs are the leading energy storage solutions for applications like portable electronics, electric vehicles, and renewable energy systems.[9–11] However, graphite, commonly used as the anode material in LIBs, has a low specific capacity of 372 mA h g^{-1}, which limits its ability to meet the growing demand for higher energy densities.[12,13] Graphene, a two-dimensional monolayer of sp^2-bonded carbon atoms, has gained significant attention as a material for lithium-ion batteries due to its exceptional properties, including high mechanical strength, high capacity, excellent electrical and thermal conductivity, and a very high specific surface area.[14–16]

[a]*Center for Environmental Intelligence and College of Engineering and Computer Science, VinUniversity, Hanoi 100000, Vietnam. E-mail: long.np2@vinuni.edu.vn*

[b]*Applied Physical Chemistry Laboratory (APCLab), University of Science, Vietnam National University Ho Chi Minh City (VNUHCM), Ho Chi Minh 700000, Vietnam. E-mail: lmlphung@hcmus.edu.vn*

[c]*Department of Physical Chemistry, Faculty of Chemistry, University of Science, Ho Chi Minh 700000, Vietnam*

† These authors contributed equally to this work.

Open Access Article. Published on 19 May 2025. Downloaded on 1/20/2026 8:11:44 AM. This article is licensed under a Creative Commons Attribution-NonCommercial 3.0 Unported Licence.

However, the aggregation and restacking of graphene sheets, caused by intersheet van der Waals forces, significantly compromise their unique properties, which leads to rapid capacity fading.[17] Generally, one of the best strategies to avoid aggregation and restacking is to add some spacer between the graphene sheets. In the meantime, the spacer could best contribute to the active material's overall surface area, conductivity, and specific capacity.[14,18]

Nanostructured transition-metal oxides are promising candidates for spacers due to their high theoretical capacities, environmental friendliness, and cost-effectiveness.[19] Among these, manganese dioxide (MnO_2) stands out for its high theoretical capacity (1230 mA h g^{-1}), low price, and environmental friendliness.[20] However, limitations such as volume expansion and particle polymerization can lead to particle pulverization and reduced inter-particle contact, leading to electrode degradation.[19] Additionally, MnO_2's low electrical conductivity (10^{-5} to 10^{-6} S cm^{-1})[21] results in a substantial capacity decline at high current densities, contributing to irreversible capacity loss and decreased cycling stability over time.[22]

This work explores recycling the graphite electrode from waste Zn–C batteries to produce low-cost GNs. Afterward, GNs@MnO_2 composite will be synthesized using an oxidation–reduction strategy. The combination of GNs and MnO_2 is expected to create a composite that can overcome the limitations of each material and have enhanced performance in lithium-ion batteries. In this study, the ultrathin MnO_2 nanosheets are decorated on graphene oxide nanosheets to obtain a two-dimensional composite to improve the electrochemical storage ability of lithium-ion battery applications. GNs work as an electron highway to increase the electrical conductivity of the electrode. In addition, the GNs layers can prevent the aggregation of MnO_2 nanoparticles and the volume expansion/contraction during the charge and discharge process. Moreover, the uniform distribution of metal oxide on graphene oxide nanosheets can avoid restacking the graphene oxide sheets.

2 Experimental

2.1 Materials

Carbon rods were obtained from spent zinc–carbon batteries, while table salt was sourced from a local supermarket. Manganese(II) chloride ($MnCl_2$), potassium permanganate ($KMnO_4$), polyvinylidene fluoride (PVDF), and *N*-methyl-2-pyrrolidone (NMP) were purchased from Sigma-Aldrich. Conductive carbon C65 was purchased from Imerys.

2.2 Preparation of graphene oxide nanosheets

Graphene oxide nanosheets were synthesized using a simple and rapid electrochemical exfoliation method. First, two carbon rods were used as the anode and cathode, with a 10% table salt solution as the aqueous electrolyte. The electrochemical exfoliation was conducted by applying a DC voltage of 3.5 V for three days, resulting in a black mixture. The mixture was then filtered, washed multiple times with deionized water, and dried at 80 °C for three days to yield graphene oxide powder.

Table 1 MnO_2 mass percent in GNs@MnO_2 composites

Sample	n_{MnO_2} (mol)	m_{MnO_2} (g)	m_{MnO_2} (%)
GM0025	5×10^{-4}	0.0435	17.86
GM005	1×10^{-3}	0.087	30.31
GM01	2×10^{-3}	0.174	46.52

2.3 Preparation of GNs@MnO_2

The MnO_2-decorated graphene oxide nanosheets were synthesized using a simple oxidation–reduction method. In this process, three different concentrations of $KMnO_4$ solution (0.0025 M, 0.005 M, and 0.01 M) were prepared, each in 200 mL of solution and transferred into separate burets. Simultaneously, 200 mg of graphene oxide was mixed with 200 mL of a 1 : 1 volume ratio of ethanol, deionized water, and sonicated for 2 hours to obtain a homogeneous grey dispersion. Each $KMnO_4$ solution was then slowly added dropwise into the respective graphene oxide mixtures while stirring vigorously at 700 rpm until the entire $KMnO_4$ solution was incorporated. The resulting mixtures were stirred continuously for 24 hours, and then allowed to stabilize for an additional 24 hours. The final products were labeled GM0025, GM005, and GM01 corresponding to the different $KMnO_4$ concentrations used (Table 1).

Fig. 1 illustrates the process of preparing MnO_2 nanosheets decorated on graphene oxide nanosheets through a simple oxidation–reduction reaction. The following equation can describe the chemical reaction involved in the formation of MnO_2:[23,24].

$$KMnO_4 + C_2H_5OH \rightarrow MnO_2 + CH_3COOH + KOH + H_2O \quad (1)$$

This method for synthesizing MnO_2 nanosheets offers several advantages, including consistent product quality, short processing time, ease of implementation and control, scalability, and cost-effectiveness.

$$n_{MnO_2} = n_{KMnO_4} = C_{M\ ddKMnO_4} \times V_{ddKMnO_4} = C_{M\ ddKMnO_4} \times 0.2$$

$$\%\, m_{MnO_2} = \frac{m_{MnO_2}}{m_{MnO_2} + m_{\text{graphene oxide nanosheets}}} = \frac{m_{MnO_2}}{m_{MnO_2} + 0.2}$$

2.4 Materials characterization and electrochemical measurements

The morphology and structure of GNs@MnO_2 composites were investigated by X-ray diffraction (XRD, D2 Bruker), Raman spectroscopy (Horiba), and scanning electron microscopy (SEM, Hitachi S-4800) and high-resolution transmission electron microscopy (HR-TEM, JEM2100).

The anode material was prepared by blending GNs@MnO_2 composites (four samples: GNs, GM0025, GM005, GM01) (80 wt%), C65 (5 wt%), and binder PVDF (15 wt%). The electrode slurry was made by mixing these components with NMP to form a homogeneous dispersion. The slurry was then coated onto

© 2025 The Author(s). Published by the Royal Society of Chemistry

Open Access Article. Published on 19 May 2025. Downloaded on 1/20/2026 8:11:44 AM.
This article is licensed under a Creative Commons Attribution-NonCommercial 3.0 Unported Licence.

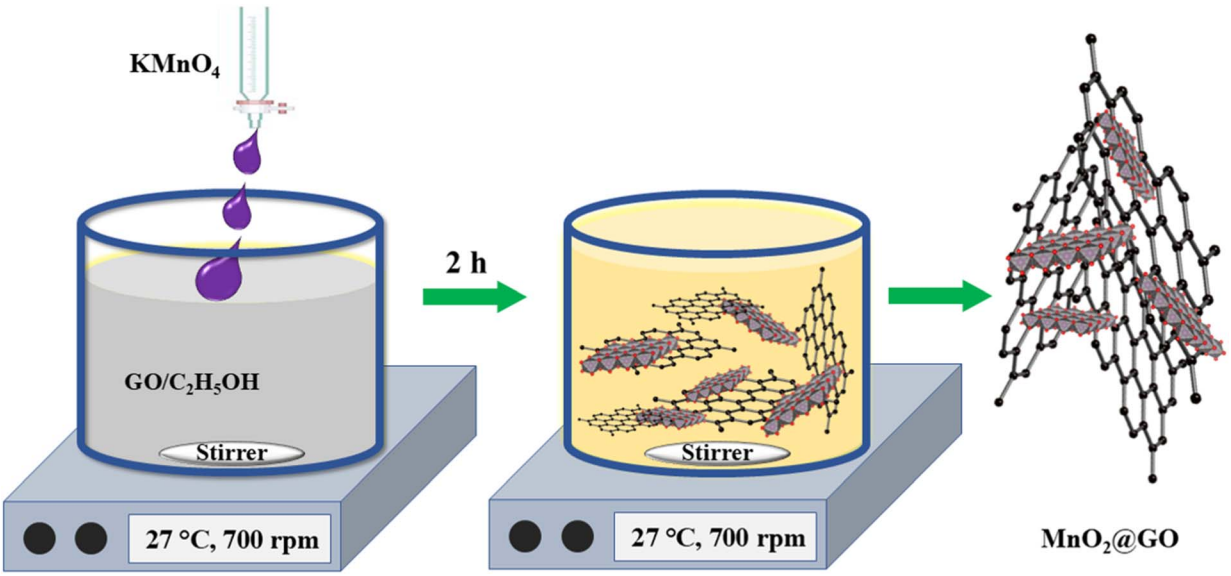

Fig. 1 The process of synthesizing MnO_2@GNs composite.

copper foil using the Doctor Blade technique and dried in a vacuum at 80 °C for 8 hours. After drying, the electrode film was punched into discs with a diameter of 12.7 mm and a mass loading of 3–3.5 mg cm^{-2}. CR2032 half-cells were assembled in an argon-filled glove box (MB20G, MBRAUN) with oxygen and moisture levels below 1 ppm. The cells utilized a polyethylene (PE) separator (Sigma-Aldrich) and an electrolyte consisting of 1.0 M $LiPF_6$ in EC : DMC (1 : 1 – v/v) mixture with 2 wt% FEC (Fluoroethylene carbonate, 99%, Sigma-Aldrich). Lithium metal was used as the counter electrode.

The anode material was made by blending GNs@MnO_2 composites (four samples: GNs, GM0025, GM005, GM01) (80% wt), C65 (5% wt), and PVDF (15% wt.) as a binder. The electrode slurry was prepared by mixing these components in NMP to achieve a homogenous mixture. This mixture was then coated onto a Cu foil using the Doctor Blade method and dried in a vacuum at 80 °C for 8 hours. Subsequently, the electrode film was punched into a round shape with a diameter of 12.7 mm and a mass loading of 3–3.5 mg cm^{-2}.

CR2032 half-cells were assembled in an argon-filled glove box (MB20G, MBRAUN) with oxygen and water maintained below 1 ppm. The cells used a PE separator (polyethylene, Sigma Aldrich) and 1.0 M $LiPF_6$ in EC : DMC (1 : 1 – v/v) with 2 wt% FEC (Fluoroethylene carbonate, 99%, Sigma-Aldrich) as the electrolyte. Lithium metal served as a counter electrode.

The Li‖GNs@MnO_2 half-cells were tested within a voltage range of 0.01–3.0 V (*vs.* Li^+/Li) at a discharge rate of 0.1 A g^{-1} and a charge rate of 0.5 A g^{-1}, following five discharge/charge cycles at 0.1 A g^{-1}. For rate performance testing, the half-cells were discharged at 0.1 A g^{-1} and then charged at varying rates (0.05, 0.1, 0.2, 0.5, 1.0, 2.0, 5.0 A g^{-1}, and returning to 0.1 A g^{-1}) for five cycles at each rate. All electrochemical tests were conducted at 30 °C using Landt (China) equipment. Cyclic voltammetry (CV) was performed using an MPG-2 system (Biologic, France) at a scan rate of 0.1 mV s^{-1} over the same voltage range. Electrochemical impedance spectroscopy (EIS) measurements were carried out using a VSP instrument (Biologic, France), with an AC potential stimulus of 10 mV and a frequency range of 500 kHz to 10 MHz.

3 Results and discussions

3.1 Materials characterization

During the redox reaction, with strong magnetic stirring at 700 rpm, MnO_2 clusters of nanosheet size are formed and evenly adhere to the surface of the graphene. This process is expected to enhance the electrochemical response of the GNs@MnO_2 composites, thereby improving the battery efficiency.

Fig. 2 presents the XRD and Raman spectra of synthesized samples. XRD diffraction patterns showed the most prominent peak for the GNs, which appears around 26°, corresponding to the (002) plane of graphene oxide,[25] with a high intensity dominating the MnO_2 peak (Fig. 2a). In the nanocomposite, the graphene diffraction peak is diminished or nearly eliminated. Due to the high MnO_2 content in the GNs@MnO_2 nanocomposite, either the regularly stacked graphene layers are exfoliated, or the graphene peak is obscured by the MnO_2 diffraction peaks.[26] GM0025 (red): a smaller peak at around 37° and a larger peak at about $2\theta = \sim 28°$ are visible. GM005 (blue): likewise, there are several tiny peaks at 37° and a significant peak at about 28°. GM01 (green): there is a prominent peak at about 28°, followed by lesser peaks at about 37° and 49°. Since the emergence of the peaks at ~28° and ~49° is diagnostic of alpha-MnO_2, the samples (GM0025, GM005, GM01) are likely to correspond to the alpha-MnO_2 phase (JCPDS No. 044–0141) based on the positions of the primary peaks (~28°, 37°, and maybe 49°).[27]

The Raman spectrum (Fig. 2b) provides further insight into the structural characteristics of the sample. In the GNs sample,

Open Access Article. Published on 19 May 2025. Downloaded on 1/20/2026 8:11:44 AM.
This article is licensed under a Creative Commons Attribution-NonCommercial 3.0 Unported Licence.

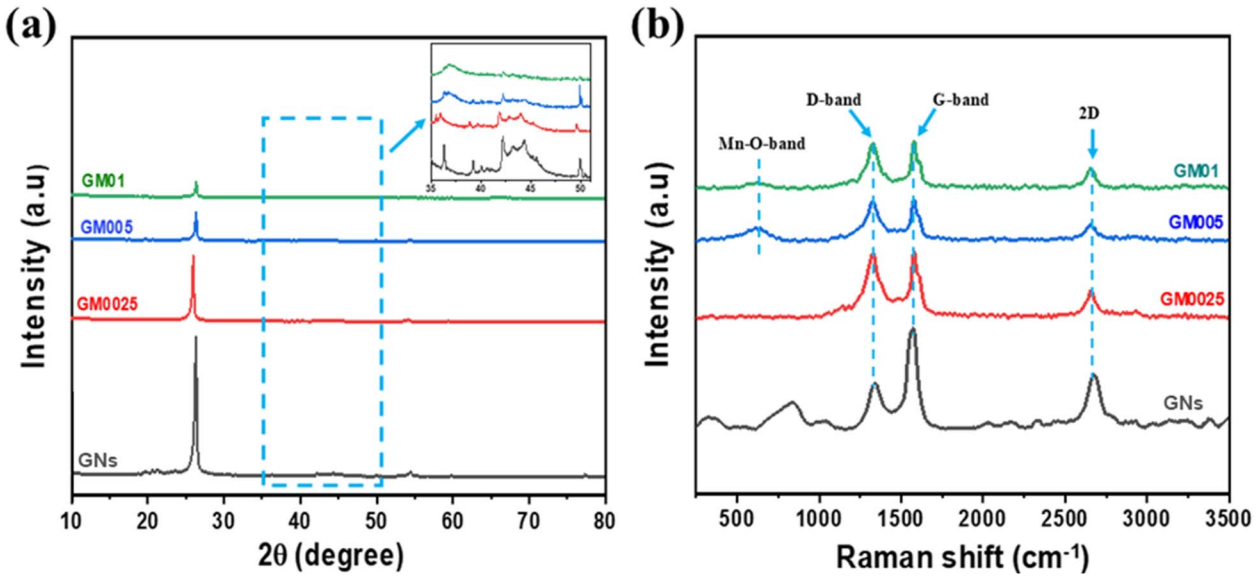

Fig. 2 (a) XRD pattern, and (b) Raman spectra of GNs@MnO_2 composites.

three main characteristic bands of graphene oxide are observed: the D band (~1326 cm^{-1}), the G band (~1573 cm^{-1}), and the 2D band (~2648 cm^{-1}). The G and D bands are related to defects in the sp^2-hybridized graphite carbon network (E_{2g} mode), while the A_{1g} mode is associated with disorder at the K point. The 2D band, which corresponds to the number of graphene oxide layers, reflects defects caused by disorder in the graphene oxide structure.[28,29] The symmetrical 2D band around 2648 cm^{-1} indicates a uniform, few-layer structure of graphene oxide nanosheets in the composite material. When MnO_2 is present, a characteristic peak appears at 614 cm^{-1}, corresponding to the Mn–O stretching vibration, confirming the presence of MnO_2.[30–32] This peak becomes more pronounced as the MnO_2 content increases, further confirming the successful deposition of MnO_2 onto the graphene oxide framework. A notable trend in the Raman spectrum is the variation in the intensity ratio of I_D/I_G, which reflects the degree of disorder in the carbon structure. This change indicates that the incorporation of MnO_2 affects the defect density in the carbon matrix, which may influence its electronic and electrochemical properties.[33] In the GM0025 sample, the D and G bands exhibit higher intensity compared to GM005 and GM01, suggesting that the distribution of GM0025 is better dispersed on the graphene oxide surface, creating more defect sites.

SEM images in Fig. 3(a and b) reveal that the electrochemical exfoliation process, using carbon rods from spent zinc–carbon batteries, produces GNs with high uniformity, few layers, and large graphene sheets at the microscale. These results suggest that the graphene oxide nanosheets have great potential for use as electrodes in electrochemical energy storage devices. Fig. 3(c–h) presents the SEM images of GNs@MnO_2 composites with varying MnO_2 content. As the concentration of $KMnO_4$ increases, more MnO_2 is deposited onto the graphene surface. The formation of MnO_2 on the surface of graphene oxide nanosheets is a result of an oxidation–reduction reaction (eqn (1)), with strong magnetic stirring during the synthesis process. This leads to the formation of nano-sized MnO_2 that adhere tightly to the graphene surface. In this configuration, graphene oxide nanosheets act as a conductive and chemically stable substrate for the MnO_2 layers. As the $KMnO_4$ concentration increases from 0.0025 M to 0.05 M and 0.1 M, the amount of MnO_2 nanosheets also increases, leading to the formation of flower-like MnO_2 structures on the graphene oxide nanosheets. This increase in MnO_2 loading is expected to enhance the electrochemical performance of the composites.

In addition, EDS analysis in the image shows the distribution of C, O and Mn elements on the material surface. In the sample containing only graphene oxide nanosheets, only two elements C and O were detected, indicating the pure structure of graphene oxide without the presence of Mn. As the MnO_2 concentration gradually increased from GM0025 to GM01, the Mn signal in the EDS spectrum became clearer, proving the success of the MnO_2 coating on the graphene oxide nanosheets surface. In the GM0025 sample, the Mn distribution density was still sparse, while in GM005, the Mn distribution became more uniform. In the GM01 sample, the Mn content increased significantly and was more concentrated, indicating the formation of large MnO_2 clusters on the material surface. This result confirmed that the increase in MnO_2 concentration had a direct effect on the coating degree and Mn distribution on graphene oxide nanosheets.

The supplied TEM images show the shape of GNs and GNs@MnO_2 (Fig. 4). The GNs in Fig. 4(a and b) show high transparency with different areas of light and dark, suggesting the existence of stacked layers. On the other hand, the GNs material after adding MnO_2 is depicted in Fig. 4(c and d), where MnO_2 nanoparticles are scattered across the GNs surface. The effective attachment of MnO_2 is further confirmed by the high-magnification Fig. 4d. The differences in contrast and morphology between the graphene and GNs@MnO_2 images

© 2025 The Author(s). Published by the Royal Society of Chemistry

Open Access Article. Published on 19 May 2025. Downloaded on 1/20/2026 8:11:44 AM.
This article is licensed under a Creative Commons Attribution-NonCommercial 3.0 Unported Licence.

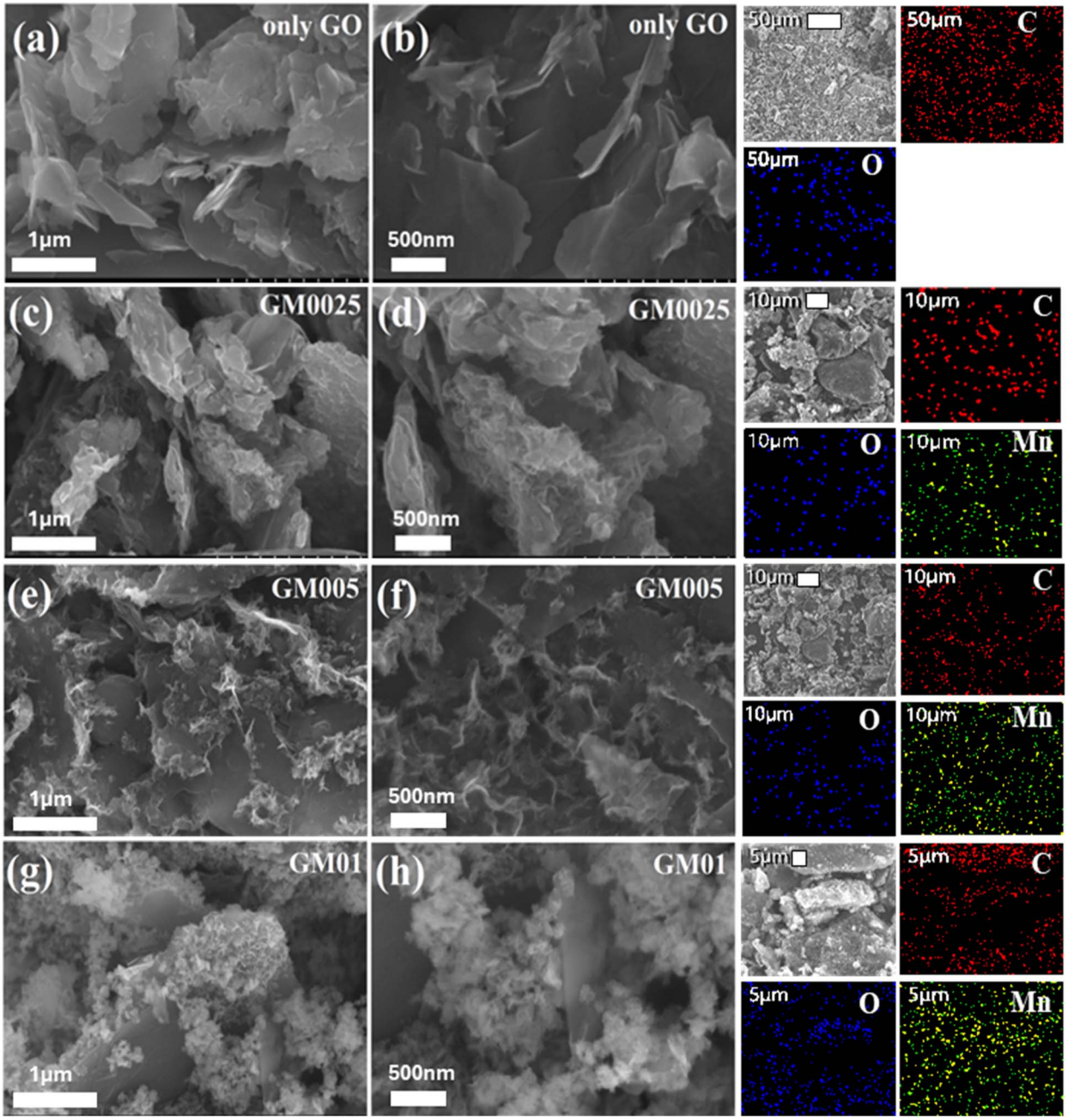

Fig. 3 SEM images of (a and b) only graphene oxide nanosheets, (c and d) GM0025, (e and f) GM005, and (g and h) GM01.

suggest that MnO_2 is well-distributed on the graphene oxide nanosheets, verifying the successful synthesis of the composite material.[34]

3.2 Electrochemical studies of lithium-ion batteries

The cyclic voltammograms (CV) of the GNs@MnO_2 composites, shown in Fig. 5(a–d), exhibit characteristic features of both GNs and MnO_2. MnO_2 shows a lithium alloying peak around 0.3–0.4 V, which corresponds to the reaction:[15,19]

$$MnO_2 + 4Li^+ + 4e^- \rightarrow Mn + 2Li_2O$$

Additionally, dealloying occurs around 1.3 V, corresponding to the oxidation of Mn to Mn^{4+}.[19] For graphene oxide nanosheets, a reduction peak is observed around 0.2 V, indicating lithium intercalation and the formation of the solid electrolyte interface (SEI) layer, while an oxidation peak around 0.3 V corresponds to the deintercalation of lithium from the Li_xC composite.[35,36]

The CV curves of the GM01 sample show distinct differences from the other samples. While higher concentrations of MnO_2 result in increased peak intensity, the GM01 sample experiences non-reversible processes, leading to structural changes and degradation during cycling. As a result, the 0.3 V peak

© 2025 The Author(s). Published by the Royal Society of Chemistry

Open Access Article. Published on 19 May 2025. Downloaded on 1/20/2026 8:11:44 AM.
This article is licensed under a Creative Commons Attribution-NonCommercial 3.0 Unported Licence.

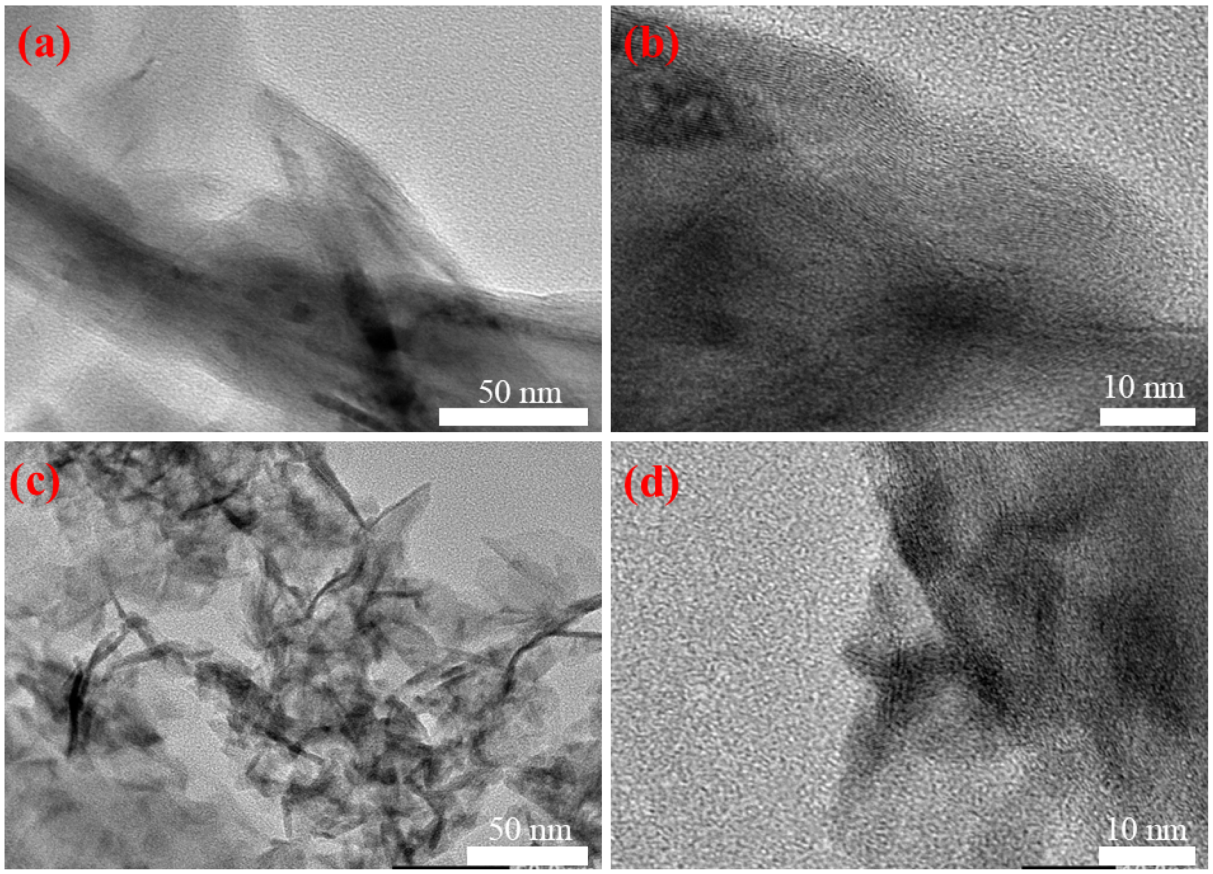

Fig. 4 TEM image of (a and b) GNs and (c and d) GM005.

associated with MnO_2 is not well-preserved in subsequent cycles. In contrast, the other samples exhibit reversible processes, allowing MnO_2 to return to its original state after each cycle. This maintains structural integrity and stable peak intensity over multiple cycles, indicating superior capacity retention and better cycling stability.

The first discharge–charge (D–C) profiles of four GNs@MnO_2 composites at a current density of 0.05 A g^{-1} are displayed in Fig. 6a. In the initial discharge process, the GNs@MnO_2 composites (GM0025, GM005, GM01) display an extended voltage plateau of around 0.5 V. This plateau gradually declines to 0.01 V, which is associated with forming the solid electrolyte interface (SEI) layer and the alloying of Li^+ into MnO_2.[15,19] In the initial charge curve of GNs and GNs@MnO_2 composites, the first voltage slope between 1.0 and 1.5 V reflects the typical voltage behavior of the MnO_2.[19] The second slope, near 0.3 V, indicates the Li^+ deintercalation process from the graphene oxide nanosheet structure.[35,36] The voltage plateaus for the first D–C profiles are consistent with the CV curves of GNs and GNs@MnO_2 electrodes in Fig. 5.

Fig. 6b illustrates the rate capability of all samples. The GNs@MnO_2 electrodes show significantly higher discharge capacities than the bare GNs electrode at all current densities, with the GM005 composite exhibiting the best performance. At 0.1 A g^{-1}, GNs delivered the lowest capacity of 283.0 mA h g^{-1}, while GM005 achieved the highest at 372.8 mA h g^{-1}. As the current density increased, GNs experienced a more pronounced capacity decline. At 5.0 A g^{-1}, GM005 maintained a capacity of 235.8 mA h g^{-1}, higher than that of GNs (194 mA h g^{-1}). When the current density was reduced back to 0.1 A g^{-1}, GNs showed only a 91.34% capacity recovery, while GM005 recovered to 118.4%. Similarly, the GM0025 composite outperformed GNs in capacity (220.4 mA h g^{-1} at 5.0 A g^{-1}) and achieved a capacity recovery of 103.2%. In contrast, the GM01 sample exhibited lower capacity than GNs at high current density (220.4 mA h g^{-1} at 5.0 A g^{-1}), though it showed better capacity recovery (102.2%).

Fig. 6c represents the cycling performance of the electrodes at a discharge rate of 0.5 A g^{-1} after the first five cycles at 0.1 A g^{-1}. Electrodes containing MnO_2 significantly improve capacity and cycling stability compared to the bare GNs electrode. In the 6th cycle, the GNs electrode exhibited a capacity of 246.4 mA h g^{-1} with a coulombic efficiency of 75.31%. It remains 99.55% after 100 cycles. Among the GNs@MnO_2 composites, the GM005 sample performed the best, with a capacity of 382.1 mA h g^{-1} and 136.83% capacity retention after 100 cycles, surpassing the bare graphene electrode. GM0025 also exhibited higher capacities and improved cycling stability than graphene, achieving capacities of 277.7 mA h g^{-1} after 100 cycles. In contrast, GM01 demonstrates the worst

© 2025 The Author(s). Published by the Royal Society of Chemistry

Open Access Article. Published on 19 May 2025. Downloaded on 1/20/2026 8:11:44 AM.
This article is licensed under a Creative Commons Attribution-NonCommercial 3.0 Unported Licence.

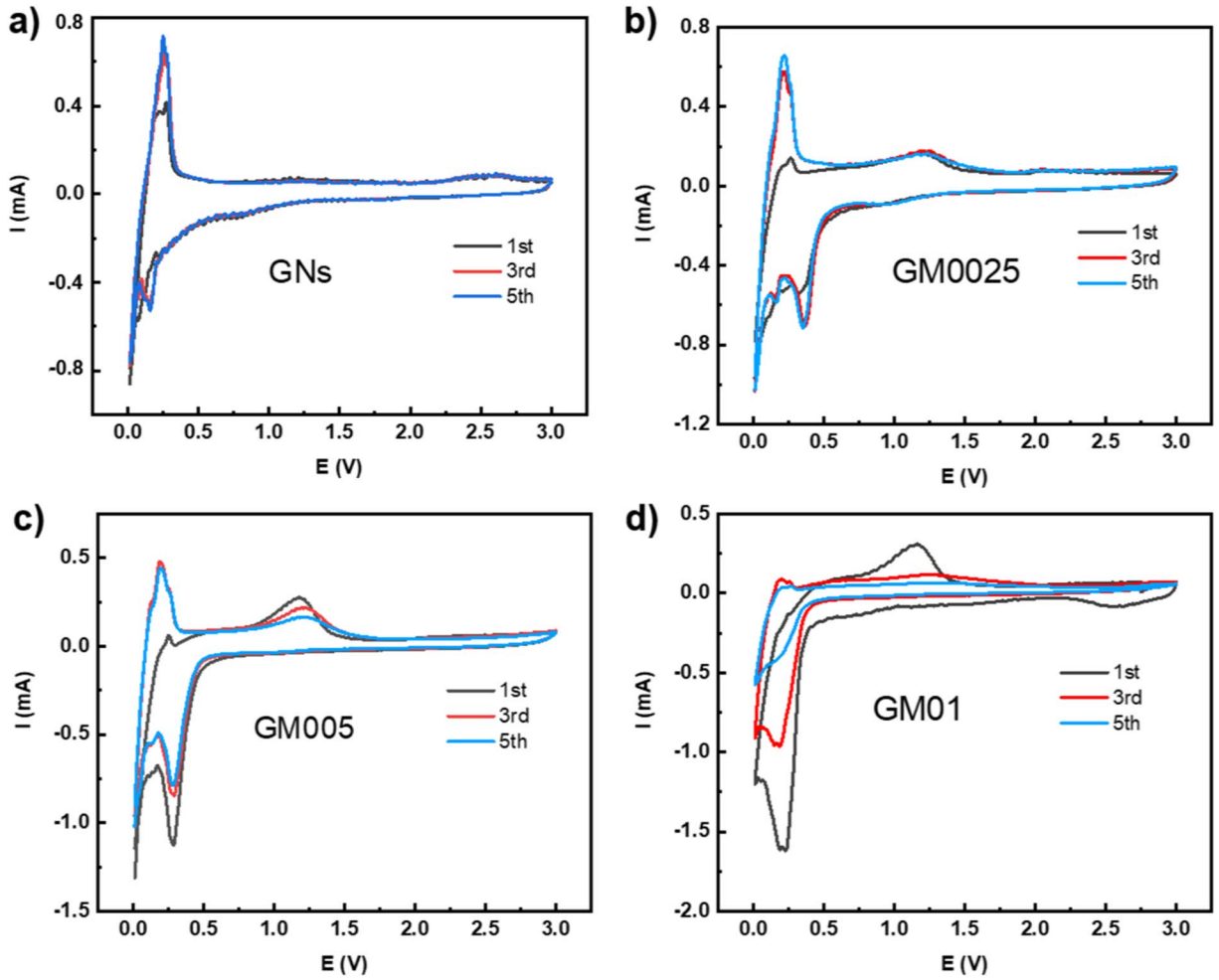

Fig. 5 CV curves of (a) GNs, (b) GM0025, (c) GM005, and (d) GM01.

performance, with the lowest capacity among all samples, at 185.6 mA h g^{-1} after 100 cycles. The relatively poor capacity in GM01 can be attributed to the loss of electrical contact between particles due to significant volume changes during Li-ion insertion and extraction.[19] After several cycles, the capacity of the GNs@MnO_2 composites increased. Initially, capacity decreased due to the pulverization and loss of connectivity during lithiation. However, later cycles showed increased capacity as the crystalline MnO_2 transitioned into a more flexible, amorphous structure, better accommodating volume changes despite ongoing electrochemical isolation.[20,37]

The GNs@MnO_2 composites perform well at high current densities with excellent capacity recovery thanks to their synergistic effects. These can be summarized in four key factors. First, MnO_2 has a high theoretical capacity for lithium storage (1230 mA h g^{-1}), which enhances the overall capacity of the composite.[20] Second, GNs provide high electrical conductivity, facilitating electron transfer during the redox reactions of MnO_2 and improving overall reaction kinetics.[19,20] Third, the structural flexibility of GNs helps absorb volumetric changes during lithiation and delithiation, preventing MnO_2 from stacking or pulverizing.[19,38] Fourth, MnO_2 anchored to the surface of GNs helps prevent the sheets from restacking, preserving the active surface area of the material.[14,38,39]

However, the GM01 sample experienced the most significant capacity loss, corresponding with the irreversible processes during subsequent cycles in Fig. 5. The Electrochemical Impedance Spectroscopy (EIS) results in Fig. 6d will explain why the GM01 sample shows the lowest capacity among the GNs@MnO_2 composites. The equivalent circuit used for modeling includes R_s, representing the bulk resistance, and two series-connected units, each consisting of a resistance parallel with a constant-phase element (CPE) and a Warburg diffusion element (W_o). The subscripts SEI and ct refer to the solid electrolyte interphase film and charge transfer resistance.[40,41]

As summarized in Table 2, as the MnO_2 content increases, both the charge transfer resistance and bulk resistance of the cell rise due to the inherently low electrical conductivity of MnO_2. In contrast, GNs provide excellent electrical conductivity and high electron mobility.[16] The GNs coating enhances the electrode's conductivity, facilitating efficient electron transport during lithium insertion and extraction.[19] The overall conductivity improves as the graphene content increases in the GNs@MnO_2 composites. The GM0025 sample shows the lowest

Open Access Article. Published on 19 May 2025. Downloaded on 1/20/2026 8:11:44 AM.
This article is licensed under a Creative Commons Attribution-NonCommercial 3.0 Unported Licence.

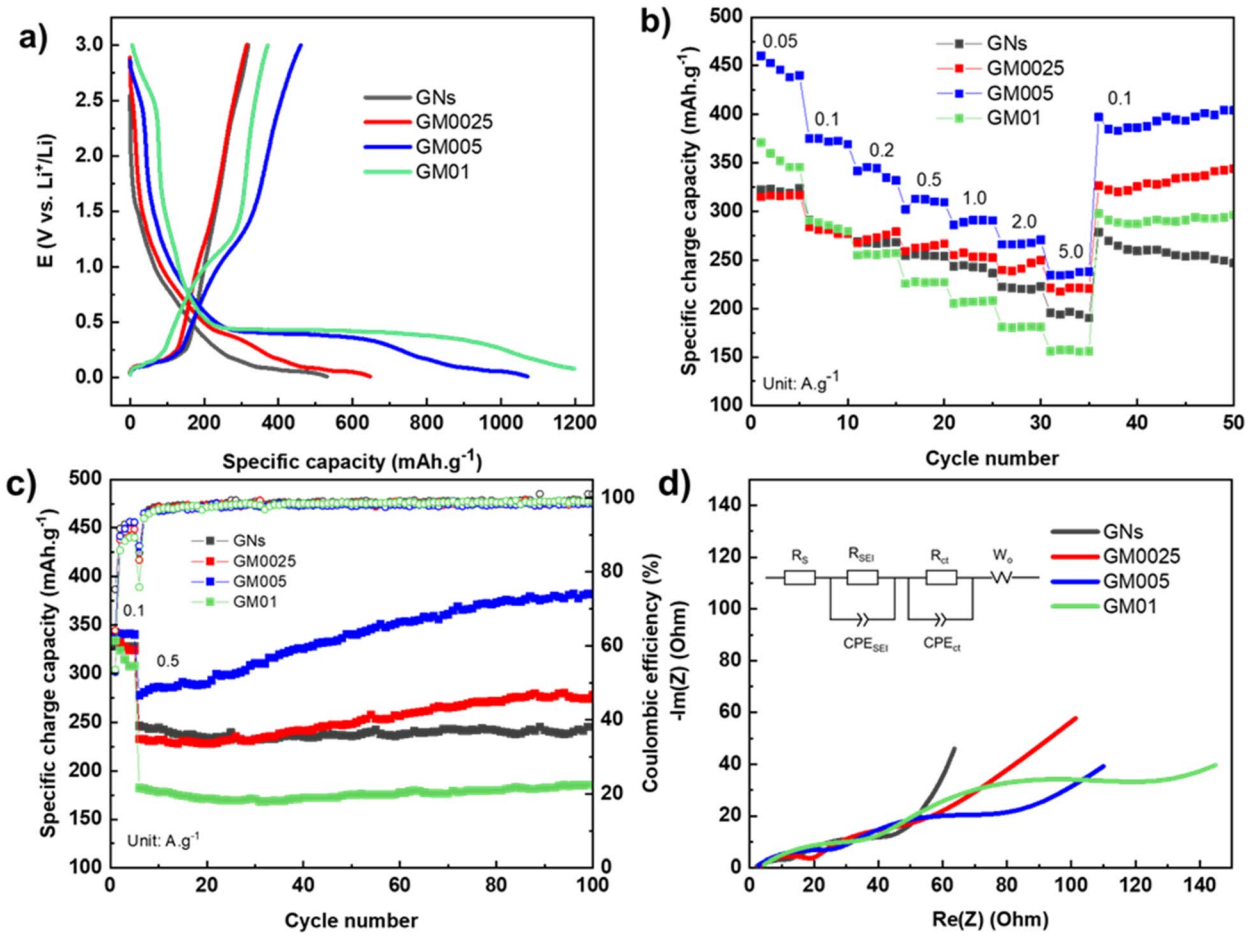

Fig. 6 (a) Voltage profile at 1st cycle, (b) rate capability, (c) cycling performance, and (d) Nyquist plot of EIS after 25 cycles of GNs and all GNs@MnO_2 samples.

Table 2 The fitting EIS results of GNs and GNs@MnO_2 samples after 25 cycles

Sample	R_s (Ω)	R_{SEI} (Ω)	R_{ct} (Ω)
GNs	2.432	9.498	30.8
GM0025	2.912	17.7	31.18
GM005	1.62	28.91	50.64
GM01	3.134	42.31	81.2

total resistance, while the GM01 electrode exhibits the highest resistance. This suggests that the GM01 electrode has the poorest electrical conductivity, which correlates with its lower reversible capacity than the other samples.

Two main factors can explain the superior capacity increase of GM005 during cycling compared to GM0025 and GM01. First is the optimal composition of MnO_2 and graphene oxide nanosheets (GNs). GM005 achieves a balanced ratio between MnO_2 and GNs. In GM0025, the MnO_2 content is too low, resulting in insufficient active sites for Li^+ storage. Since MnO_2 has a much higher theoretical capacity (1230 mA h g^{-1})[20] than graphene oxide (540 mA h g^{-1}),[16] this limits the capacity of GM0025. On the other hand, GM01 contains an excessive amount of MnO_2, which leads to agglomeration and reduces the effective contact area with the electrolyte. Additionally, the lowest GNs content in GM01 causes the highest resistance (R) among all GNs@MnO_2 samples (Fig. 6d and Table 2), making electron transport less efficient. Second, GM005 has better MnO_2 dispersion and structural integrity. SEM images (Fig. 3) show that the MnO_2 in GM005 is uniformly distributed on the surface of the GNs, avoiding large aggregates. In contrast, GM0025 shows sparse MnO_2 coverage, while GM01 exhibits severe MnO_2 clustering. The homogeneous distribution in GM005 ensures a larger active surface area, better contact with the electrolyte, and improved Li^+ insertion, all contributing to its enhanced cycling performance.

Based on GM005's best results, XPS was used to examine this sample's compositional and surface chemical states further. Fig. 7a illustrates the C 1s core level XPS spectra of MnO_2 nanosheets decorating on graphene oxide nanosheets. The peak fitting was performed with the following peak component assignment: C–C at 284.6 eV (peak C1), C–O at 286.2 eV (peak C2), C═O at 288.3 eV (peak C3), COOH at 292.6 eV (peak C4), and π–π* shake up satellite, respectively.[42–44]

Fig. 7b shows the O 1s core level XPS spectra of the GM005 sample. O 1s spectra illustrate three components at 529.7 (peak

© 2025 The Author(s). Published by the Royal Society of Chemistry

Open Access Article. Published on 19 May 2025. Downloaded on 1/20/2026 8:11:44 AM.
This article is licensed under a Creative Commons Attribution-NonCommercial 3.0 Unported Licence.

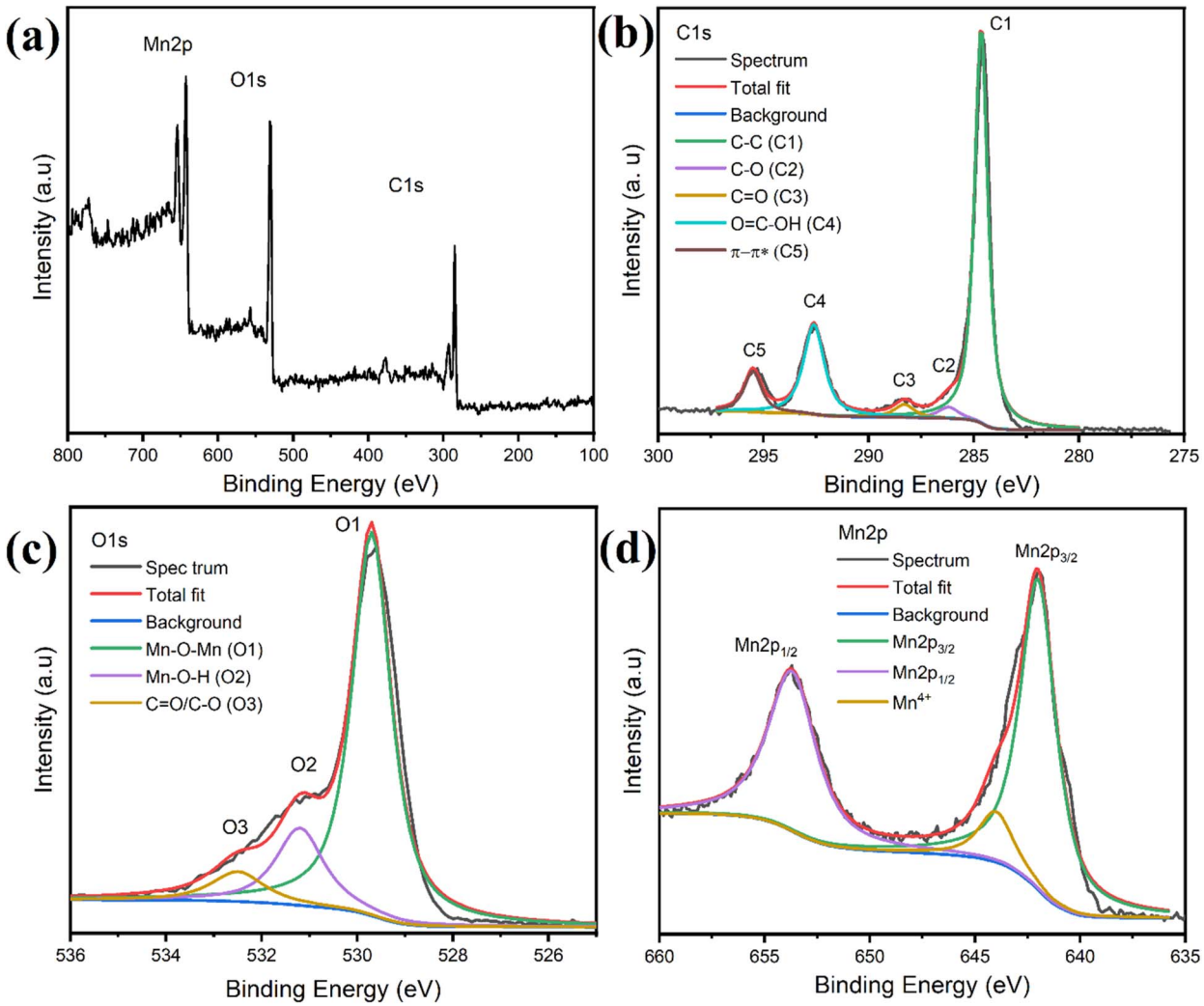

Fig. 7 XPS spectra of GNs@MnO_2 composites sample GM005: (a) survey spectrum, (b) C 1s, (c) O 1s, and (d) Mn 2p XPS spectrum.

O1), 531.2 (peak O2), and 532.5 eV (peak O3) corresponding to Mn–O, MnOH, and C–O/C═O, respectively. The XPS spectra of Mn 2p for the MnO_2 nanosheets in Fig. 7d were simulated using three sets of curves colored by pink, green, and dark yellow, respectively, to get comprehensive information on the existence of the element manganese. Fig. 7d shows the Mn 2p XPS spectra with two distinct separate peaks located at around 642 and 653.7 eV corresponding to Mn^{3+} in the composite samples, which belong to the Mn $2p_{1/2}$ of the high-energy band and Mn $2p_{3/2}$ of the low-energy band, respectively.[45,46] Moreover, the spin energy separation of 11.7 eV between Mn $2p_{1/2}$ and Mn $2p_{3/2}$ indicates the existence of Mn^{4+} in the samples, which appears by dark yellow peaks at around 644 eV.[46,47] In the instance of α-MnO_2, the existence of Mn^{3+} and Mn^{4+} indicates that the manganese groups on the surface are partly reduced. More oxygen vacancies result from the MnO_2 generally larger Mn^{3+} ratio, which is very advantageous for increasing the electrochemical activity.

Table 3 highlights synthesis approaches, graphene oxide (GO) sources, and electrochemical performance, with a focus on the sustainability aspect of the present study. Due to two main factors, the GNs@MnO_2 composites synthesized in this work delivered lower specific capacity than some previously reported MnO_2/Graphene-based composite systems.

First, MnO_2 was synthesized at room temperature *via* a mild oxidation–reduction reaction without post-synthesis thermal treatment or structural tuning. While this approach avoids energy-intensive steps, it may limit the crystallinity and uniform dispersion of MnO_2 on the GO surface, resulting in only a fraction of the active material effectively contributing to lithium storage. Second, the graphene oxide used in the composite was not reduced. Although unreduced GO offers good dispersion stability, it has low electrical conductivity compared to reduced graphene oxide (rGO), which hinders electron transport.[51]

Nonetheless, the synthesis strategy in this work demonstrates the feasibility of producing electrode materials from low-cost, recycled resources with minimal chemical usage. The resulting composite still shows promising electrochemical activity and good structural integrity. These results provide a strong foundation for future optimization, such as applying

Open Access Article. Published on 19 May 2025. Downloaded on 1/20/2026 8:11:44 AM.
This article is licensed under a Creative Commons Attribution-NonCommercial 3.0 Unported Licence.

Table 3 Summary of the anode performance of MnO_2/graphene-based material composites in lithium-ion batteries

Material	Raw graphene source	Synthesis method	% MnO_2	Specific capacity	References
GNs@MnO_2	Carbon rods from used Zn–C batteries	GNs: electrochemical exfoliation GNs@MnO_2: wet chemical with $KMnO_4$	30.31	0.1 A g^{-1}: 382.1 mA h g^{-1} (100 cycles) 5.0 A g^{-1}: 235.8 mA h g^{-1}	This work
Graphene/MnO_2 nanotubes	Commercial graphite powder	Graphene: modified Hummers' method MnO_2 nanotubes: hydrothermal with $KMnO_4$ Graphene/MnO_2 nanotubes: layer-by-layer assembly	50	0.1 A g^{-1}: 495 mA h g^{-1} (40 cycles) 1.6 A g^{-1}: 208 mA h g^{-1}	48
Graphene/α-MnO_2	Commercial graphite powder	Graphene: modified Hummers' method α-MnO_2 nanowires: hydrothermal with $KMnO_4$ and $MnSO_4 \cdot H_2O$ Graphene/α-MnO_2: sonication and hydrothermal synthesis	85	0.06 A g^{-1}: 998 mA h g^{-1} (30 cycles) 12 A g^{-1}: 590 mA h g^{-1}	19
α-MnO_2/GNs	Commercial bulk graphene	Graphene nanosheets (GNs): solvothermal α-MnO_2/GNs: wet-chemical with $KMnO_4$, Na_2SO_4, SDS in GNS dispersion	~40	C/10: ~600 mA h g^{-1} (20 cycles) C/5: 387.7 mA h g^{-1} (30 cycles)	15
MnO_2@graphene	Commercial graphite powder	MnO_2 particles: hydrothermal with $MnSO_4$ and $KMnO_4$ Graphene oxide (GO): modified Hummers' method MnO_2@graphene: ultrasonication method	~80	50 mA g^{-1}: 1576.2 mA h g^{-1} (100 cycles) 1 A g^{-1}: ~100 mA h g^{-1}	37
MnO_2 nanotubes/ reduced graphene oxide (MnO_2/RGO)	Commercial graphite powder	Graphene oxide (GO): modified Hummers' method MnO_2 nanotubes: hydrothermal with $KMnO_4$ and HCl MnO_2/RGO membranes: ultrasonication and thermal reduction	49	0.1 A g^{-1}: 1006.7 mA h g^{-1} (100 cycles) 2 A g^{-1}: 202.5 mA h g^{-1}	46
MnO_2/graphene nanocomposites	Commercial graphite powder	Graphene oxide (GO): modified Hummers' method MnO_2/GO: hydrothermal with GO, $MnCl_2 \cdot 4H_2O$ and urea	~80	0.1 A g^{-1}: 750.24 mA h g^{-1} (50 cycles) 1 A g^{-1}: 476.4 mA h g^{-1}	38
MnO_2 nanorods/ reduced graphene oxide (rGO)	Commercial flake graphite	Graphene oxide: modified Hummers' method MnO_2 nanorods: hydrothermal synthesis using $KMnO_4$ and $MnSO_4 \cdot H_2O$, modification with APTES MnO_2/rGO: hydrothermal synthesis	50	0.5 A g^{-1}: ~600 mA h g^{-1} (650 cycles) 5 A g^{-1}:168.2 mA h g^{-1}	49
δ-MnO_2 nanoscrolls/ RGO	Commercial natural graphite	Graphene oxide: modified Hummers' method RGO: reduction with ascorbic acid δ-MnO_2 nanoscroll/RGO: hydrothermal with $KMnO_4$, HCl, and RGO dispersion	~90	0.1 A g^{-1}: 528 mA h g^{-1} (50 cycles) 1 A g^{-1}: 226 mA h g^{-1}	50

© 2025 The Author(s). Published by the Royal Society of Chemistry

Open Access Article. Published on 19 May 2025. Downloaded on 1/20/2026 8:11:44 AM. This article is licensed under a Creative Commons Attribution-NonCommercial 3.0 Unported Licence.

hydrothermal treatment at elevated temperatures. This step could simultaneously enhance the crystallinity and uniform distribution of MnO_2 on graphene-based material while partially reducing GO to rGO, thereby improving both structural integration and electrical conductivity.[49–52] Such improvements are expected to bring this sustainable approach closer to practical applications in lithium-ion batteries.

4 Conclusions

This study offered a novel material from carbon rods from spent Zn–C batteries. The process involved synthesizing graphene oxide nanosheets (GNs) through a simple one-step electrochemical exfoliation. Manganese dioxide (MnO_2) was also applied to the graphene oxide nanosheets using a quick and straightforward wet-chemical method. Among the samples tested, the optimal GNs@MnO_2 composite (GM005) exhibits high cycling performance (~328 mA h g^{-1} after 100 cycles at 0.5 A g^{-1}) and good high-rate performance (~236 mA h g^{-1} at 5.0 A g^{-1}). The excellent electrochemical performance of this nanocomposite stems from the synergistic effects of GNs and MnO_2 nanoparticles. GNs prevent MnO_2 aggregation and enhance the composite's electrical conductivity. MnO_2 boosts capacity due to its high theoretical capacity and avoids restacking the graphene oxide nanosheets layers, improving the effective surface area. This research presents a practical method for synthesizing GNs@MnO_2 composite materials from electronic waste for energy storage devices.

Data availability

Data for this article, including raw experimental measurements, electrochemical performance data, and material characterization results, are available at Zenodo at **https://doi.org/10.5281/zenodo.15400523**.

Author contributions

Y. K. N. C.: and V. V. T. contribute equally to this work. Y. K. N. C.: methodology, formal analysis, investigation, data curation, writing – original draft, writing – review & editing, visualization. V. V. T.: formal analysis, investigation, data curation, writing – original draft, writing – review & editing, visualization. T. T. T. V.: investigation. V. X. N.: investigation. P. T. V.: writing – original draft, writing – review & editing. T. V. B. P.: writing – original draft, writing – review & editing, conceptualization, supervision. P. L. N.: writing – review & editing, conceptualization, supervision, project administration, funding acquisition. P. M. L. L.: writing – review & editing, conceptualization, supervision, project administration, funding acquisition.

Conflicts of interest

The authors declare that they have no known competing financial interests.

Acknowledgements

This work is financially supported by Vin University Center for Environmental Intelligence under Flagship Project VUNI.-CEI.FS_0005 and VUNI.CEI.FS_0006.

References

1 G. Sperandio, I. M. Junior, E. Bernardo and R. Moreira, Graphene Oxide from Graphite of Spent Batteries as Support of Nanocatalysts for Fuel Hydrogen Production, *Processes*, 2023, **11**, 3250, DOI: **10.3390/pr11113250**.

2 I. Roy, G. Sarkar, S. Mondal, D. Rana, A. Bhattacharyya, N. R. Saha, A. Adhikari, D. Khastgir, S. Chattopadhyay and D. Chattopadhyay, Synthesis and characterization of graphene from waste dry cell battery for electronic applications, *RSC Adv.*, 2016, **6**, 10557–10564, DOI: **10.1039/c5ra21112c**.

3 P. A. Le, N. T. Nguyen, P. L. Nguyen and T. V. B. Phung, Minireview on Cathodic and Anodic Exfoliation for Recycling Spent Zinc-Carbon Batteries To Prepare Graphene Material: Advances and Outlook of Interesting Strategies, *Energy Fuels*, 2023, **37**(10), 7062–7070, DOI: **10.1021/acs.energyfuels.3c00838**.

4 W. S. Hummers and R. E. Offeman, Preparation of Graphitic Oxide, *J. Am. Chem. Soc.*, 1958, **80**, 1339, DOI: **10.1021/ja01539a017**.

5 B. Ulrich Hofmann, The formation of salts from graphite by strong acids, *Trans. Faraday Soc.*, 1938, **34**, 1017–1021, DOI: **10.1039/TF9383401017**.

6 L. Li, D. Zhang, J. Deng, J. Fang and Y. Gou, Review—Preparation and Application of Graphene-Based Hybrid Materials through Electrochemical Exfoliation, *J. Electrochem. Soc.*, 2020, **167**, 086511, DOI: **10.1149/1945-7111/ab933b**.

7 F. Liu, C. Wang, X. Sui, M. A. Riaz, M. Xu, L. Wei and Y. Chen, Synthesis of graphene materials by electrochemical exfoliation: Recent progress and future potential, *Carbon Energy*, 2019, **1**, 173–199, DOI: **10.1002/cey2.14**.

8 S. J. Paul, P. Chandra, N. Kumar and R. Khan, Electrochemical Exfoliation of Graphene and Its Derivatives and Its Extended Applications in Therapeutics, *Eng. Mater.*, 2024, **F2883**, 263–281, DOI: **10.1007/978-981-97-2128-3_10**.

9 D. Sun, X. Yan, J. Yang, P. Zhang and Q. Xue, Hierarchically Porous and Nitrogen-Doped Graphene-Like Microspheres as Stable Anodes for Lithium-Ion Batteries, *Chemelectrochem*, 2015, **2**, 1830–1838, DOI: **10.1002/celc.201500145**.

10 D. Deng, Li-ion batteries: Basics, progress, and challenges, *Energy Sci. Eng.*, 2015, **3**, 385–418, DOI: **10.1002/ese3.95**.

11 V. Etacheri, R. Marom, R. Elazari, G. Salitra and D. Aurbach, Challenges in the development of advanced Li-ion batteries: A review, *Energy Environ. Sci.*, 2011, **4**, 3243–3262, DOI: **10.1039/c1ee01598b**.

12 N. Takami, A. Satoh, T. Ohsaki and M. Kanda, *Lithium Insertion and Extraction for High-Capacity Disordered Carbons with Large Hysteresis*, Elsevier Science Ltd, 1997.

Open Access Article. Published on 19 May 2025. Downloaded on 1/20/2026 8:11:44 AM. This article is licensed under a Creative Commons Attribution-NonCommercial 3.0 Unported Licence.

13 M. Endo, Y. Nishimurat, T. Takahashis, K. Takeuchi and M. S. Dresselhauss, Lithium Storage Behavior For Various Kinds Of Carbon Anodes In Li Ion Secondary Battery, *J. Phys. Chem. Solids*, 1996, **57**(6–8), 725–728, DOI: **10.1016/0022-3697(95)00339-8**.

14 X. Dai, W. Shi, H. Cai, R. Li and G. Yang, Facile preparation of the novel structured α-MnO2/Graphene nanocomposites and their electrochemical properties, *Solid State Sci.*, 2014, **27**, 17–23, DOI: **10.1016/j.solidstatesciences.2013.11.003**.

15 L. Xing, C. Cui, C. Ma and X. Xue, Facile synthesis of α-MnO2/graphene nanocomposites and their high performance as lithium-ion battery anode, *Mater. Lett.*, 2011, **65**, 2104–2106, DOI: **10.1016/j.matlet.2011.04.093**.

16 M. R. Al Hassan, A. Sen, T. Zaman and M. S. Mostari, Emergence of graphene as a promising anode material for rechargeable batteries: a review, *Mater. Today Chem.*, 2019, **11**, 225–243, DOI: **10.1016/j.mtchem.2018.11.006**.

17 E. R. Ezeigwe, M. T. T. Tan, S. Khiew and C. Wee Siong, Solvothermal synthesis of graphene-MnO2 nanocomposites and their electrochemical behavior, *Ceram. Int.*, 2015, **41**(9), 11418–11427, DOI: **10.1016/j.ceramint.2015.05.105**.

18 Y. Wang, Y. Wu, Y. Huang, F. Zhang, X. Yang, Y. Ma and Y. Chen, Preventing graphene sheets from restacking for high-capacitance performance, *J. Phys. Chem. C*, 2011, **115**, 23192–23197, DOI: **10.1021/jp206444e**.

19 Y. Zhang, H. Liu, Z. Zhu, K. W. Wong, R. Mi, J. Mei and W. M. Lau, A green hydrothermal approach for the preparation of graphene/α-MnO23D network as anode for lithium ion battery, *Electrochim. Acta*, 2013, **108**, 465–471, DOI: **10.1016/j.electacta.2013.07.002**.

20 J. H. Park, W. Y. Choi, S. Lee, T. S. Kim and J. W. Lee, Graphene intercalated free-standing carbon paper coated with MnO2 for anode materials of lithium ion batteries, *Electrochim. Acta*, 2020, **348**, 136310, DOI: **10.1016/j.electacta.2020.136310**.

21 K. F. El-Nemr, M. R. Balboul and M. A. Ali, Electrical and mechanical properties of manganese dioxide-magnetite-filled acrylonitrile butadiene rubber blends, *J. Thermoplast. Compos. Mater.*, 2016, **29**, 704–716, DOI: **10.1177/0892705714533372**.

22 H. Lai, J. Li, Z. Chen and Z. Huang, Carbon nanohorns as a high-performance carrier for MnO2 anode in lithium-ion batteries, *ACS Appl. Mater. Interfaces*, 2012, **4**, 2325–2328, DOI: **10.1021/am300378w**.

23 N. R. Chodankar, G. S. Gund, D. P. Dubal and C. D. Lokhande, Alcohol mediated growth of α-MnO2 thin films from KMnO4 precursor for high performance supercapacitors, *RSC Adv.*, 2014, **4**, 61503–61513, DOI: **10.1039/c4ra09268f**.

24 I. K. Hewavitharana, Y. Ding, K. Y. Simon Ng and D. Deng, 1-D NiO nanorods pillared 2-D MnO2 nanosheets as lithium-free cathode materials for charged-state lithium batteries, *Chem. Eng. Sci.*, 2021, **236**, 116480, DOI: **10.1016/j.ces.2021.116480**.

25 A. A. Muhsan and K. Lafdi, Numerical study of the electrochemical exfoliation of graphite, *SN Appl. Sci.*, 2019, **1**, 276, DOI: **10.1007/s42452-019-0296-8**.

26 S. Chen, J. Zhu, X. Wu, Q. Han and X. Wang, Graphene oxide-Mno2 nanocomposites for supercapacitors, *ACS Nano*, 2010, **4**, 2822–2830, DOI: **10.1021/nn901311t**.

27 C. Yang, M. Zhou and Q. Xu, Three-dimensional ordered macroporous MnO2/carbon nanocomposites as high-performance electrodes for asymmetric supercapacitors, *Phys. Chem. Chem. Phys.*, 2013, **15**, 19730–19740, DOI: **10.1039/c3cp53504e**.

28 D. Van Thanh, H. C. Chen, L. J. Li, C. W. Chu and K. H. Wei, Plasma electrolysis allows the facile and efficient production of graphite oxide from recycled graphite, *RSC Adv.*, 2013, **3**, 17402–17410, DOI: **10.1039/c3ra43084g**.

29 D. Van Thanh, L. J. Li, C. W. Chu, P. J. Yen and K. H. Wei, Plasma-assisted electrochemical exfoliation of graphite for rapid production of graphene sheets, *RSC Adv.*, 2014, **4**, 6946–6949, DOI: **10.1039/c3ra46807k**.

30 C. M. Julien, M. Massot and C. Poinsignon, Lattice vibrations of manganese oxides: Part I. Periodic structures, *Spectrochim. Acta, Part A*, 2004, **60**, 689–700, DOI: **10.1016/S1386-1425(03)00279-8**.

31 L. Wu, R. Li, J. Guo, C. Zhou, W. Zhang, C. Wang, Y. Huang, Y. Li and J. Liu, Flexible solid-state symmetric supercapacitors based on MnO2 nanofilms with high rate capability and long cyclability, *AIP Adv.*, 2013, **3**, 8, DOI: **10.1063/1.4820353**.

32 P. Sampathkumar, M. S. Monica, K. Giribabu and C. Suresh, Influence of phase structure of MnO2 for enhancing the electrochemical sensitivity of environmental pollutant chlortetracycline, *Next Mater.*, 2024, **2**, 100079, DOI: **10.1016/j.nxmate.2023.100079**.

33 A. C. Ferrari and J. Robertson, Interpretation of Raman spectra of disordered and amorphous carbon, *Phys. Rev. B: Condens. Matter Mater. Phys.*, 2000, **61**, 14095, DOI: **10.1103/PhysRevB.61.14095**.

34 C. Zhang, X. Zhu, Z. Wang, P. Sun, Y. Ren, J. Zhu, J. Zhu and D. Xiao, Facile synthesis and strongly microstructure-dependent electrochemical properties of graphene/manganese dioxide composites for supercapacitors, 2014. **http://www.nanoscalereslett.com/content/9/1/490**.

35 L. L. Tian, Q. C. Zhuang, J. Li, Y. L. Shi, J. P. Chen, F. Lu and S. G. Sun, Mechanism of intercalation and deintercalation of lithium ions in graphene nanosheets, *Chin. Sci. Bull.*, 2011, **56**, 3204–3212, DOI: **10.1007/s11434-011-4609-6**.

36 Z. Jiang, B. Pei and A. Manthiram, Randomly stacked holey graphene anodes for lithium ion batteries with enhanced electrochemical performance, *J. Mater. Chem. A*, 2013, **1**, 7775–7781, DOI: **10.1039/c3ta10457e**.

37 W. Zhang, H. Jin, Y. Du, Y. Zhang, Z. Wang and J. Zhang, Hierarchical lamellar-structured MnO2@graphene for high performance Li, Na and K ion batteries, *ChemistrySelect*, 2020, **5**, 12481–12486, DOI: **10.1002/slct.202003584**.

38 X. Y. Zhu, J. J. Li, X. L. She and L. H. Xia, MnO2/Graphene nanocomposite for use in high performance lithium-ion batteries, *Adv. Mater. Res.*, 2013, 157–160, DOI: **10.4028/www.scientific.net/AMR.709.157**.

39 Q. Jiasheng, *Graphene/Manganese Oxide Composites for Energy Storage*, 2017.

© 2025 The Author(s). Published by the Royal Society of Chemistry

Open Access Article. Published on 19 May 2025. Downloaded on 1/20/2026 8:11:44 AM.
This article is licensed under a Creative Commons Attribution-NonCommercial 3.0 Unported Licence.

40 Z. Xiang, Y. Chen, J. Li, X. Xia, Y. He and H. Liu, Submicro-sized porous SiO2/C and SiO2/C/graphene spheres for lithium ion batteries, *J. Solid State Electrochem.*, 2017, **21**, 2425–2432, DOI: **10.1007/s10008-017-3566-7**.

41 Y. K. N. Chuong, Q. N. Nguyen, M. V. Tran, P. A. Le, P. L. M. Le, V. B. T. Phung and P. T. Vu, Electrochemical Properties of C/SiO2/Graphene Nanoplatelets as High-Rate Performance Anode Material in Li-Ion Batteries, *Energy Storage*, 2024, **6**, 6, DOI: **10.1002/est2.70043**.

42 W. Yu, X. Gao, Z. Yuan, H. Liu, X. Wang and X. Zhang, Facial fabrication of few-layer functionalized graphene with sole functional group through Diels-Alder reaction by ball milling, *RSC Adv.*, 2022, **12**, 17990–18003, DOI: **10.1039/d2ra01668k**.

43 W. Xie, L. T. Weng, K. M. Ng, C. K. Chan and C. M. Chan, Defects of clean graphene and sputtered graphite surfaces characterized by time-of-flight secondary ion mass spectrometry and X-ray photoelectron spectroscopy, *Carbon*, 2017, **112**, 192–200, DOI: **10.1016/j.carbon.2016.11.002**.

44 X. Chen, X. Wang and D. Fang, A review on C1s XPS-spectra for some kinds of carbon materials, *Fullerenes, Nanotubes Carbon Nanostruct.*, 2020, 1048–1058, DOI: **10.1080/1536383X.2020.1794851**.

45 Z. Li, Y. Mi, X. Liu, S. Liu, S. Yang and J. Wang, Flexible graphene/MnO2 composite papers for supercapacitor electrodes, *J. Mater. Chem.*, 2011, **21**, 14706–14711, DOI: **10.1039/c1jm11941a**.

46 X. Zhao, G. Wang and H. Wang, Synthesis of free-standing MnO2/reduced graphene oxide membranes and electrochemical investigation of their performances as anode materials for half and full lithium-ion batteries, *J. Nanopart. Res.*, 2016, **18**, 304, DOI: **10.1007/s11051-016-3511-1**.

47 V. T. Phat, N. V. Hoang, D. V. Minh, N. T. Trung, L. M. L. Phung and T. V. Man, Understanding the electrochemical properties of Mn7O8SiO4 as promising anode material for low-cost batteries applications: Redox reation and structural failure, *Mater. Lett.*, 2022, **320**, 132231, DOI: **10.1016/j.matlet.2022.132231**.

48 A. Yu, H. W. Park, A. Davies, D. C. Higgins, Z. Chen and X. Xiao, Free-standing layer-by-layer hybrid thin film of graphene-MnO2 nanotube as anode for lithium ion batteries, *J. Phys. Chem. Lett.*, 2011, **2**, 1855–1860, DOI: **10.1021/jz200836h**.

49 Z. Ma and T. Zhao, Reduced graphene oxide anchored with MnO2 nanorods as anode for high rate and long cycle Lithium ion batteries, *Electrochim. Acta*, 2016, **201**, 165–171, DOI: **10.1016/j.electacta.2016.03.200**.

50 H. Liu, Z. Hu, L. Tian, Y. Su, H. Ruan, L. Zhang and R. Hu, Reduced graphene oxide anchored with δ-MnO2 nanoscrolls as anode materials for enhanced Li-ion storage, *Ceram. Int.*, 2016, **42**, 13519–13524, DOI: **10.1016/j.ceramint.2016.05.144**.

51 Z. Liu, R. Navik, H. Tan, Q. Xiang, R. Morales Ibarra and Y. Zhao, Graphene-based materials prepared by supercritical fluid technology and its application in energy storage, *J. Supercrit. Fluids*, 2022, **188**, 105672, DOI: **10.1016/j.supflu.2022.105672**.

52 N. Baig, I. Kammakakam, W. Falath and I. Kammakakam, Nanomaterials: A review of synthesis methods, properties, recent progress, and challenges, *Mater. Adv.*, 2021, **2**, 1821–1871, DOI: **10.1039/d0ma00807a**.